



Anatase TiO₂ mesocrystals with exposed (0 0 1) surface for enhanced photocatalytic decomposition capability toward gaseous styrene

Jiangyao Chen ^{a,c}, Guiying Li ^a, Haimin Zhang ^b, Porun Liu ^b, Huijun Zhao ^b, Taicheng An ^{a,*}

^a State Key Laboratory of Organic Geochemistry, Guangdong Key Laboratory of Environmental Resources Utilization and Protection, Guangzhou Institute of Geochemistry, Chinese Academy of Sciences, No. 511 Kehua Street, Tianhe, Guangzhou 510640, China

^b Centre for Clean Environment and Energy, Griffith University, Gold Coast Campus QLD, 4222, Australia

^c University of Chinese Academy of Sciences, Beijing 100049, China

ARTICLE INFO

Article history:

Received 20 July 2013

Received in revised form 16 October 2013

Accepted 25 October 2013

Available online 27 November 2013

Keywords:

Anatase TiO₂ mesocrystals

Solvothermal synthesis

High energy {0 0 1} facets

Photocatalytic activity

Volatile organic compounds.

ABSTRACT

Anatase TiO₂ mesocrystals with exposed (0 0 1) surface have been successfully synthesized by a facile one-step solvothermal method using NH₄F as the structure regulator in glacial acetic acid environment. The exposed (0 0 1) surface of the obtained anatase TiO₂ mesocrystal was consisted of numerous nanocrystals with exposed {0 0 1} facet. The results indicated that both the added amount of NH₄F and solvothermal reaction time played significant roles in the formation of anatase TiO₂ mesocrystals with exposed (0 0 1) surface. A possible formation mechanism of anatase TiO₂ mesocrystal with exposed (0 0 1) surface was proposed based on the experimental data. As UV active photocatalysts, the resultant anatase TiO₂ mesocrystals were evaluated in detail by photocatalytic decomposition of gaseous styrene. The results demonstrated that the anatase TiO₂ mesocrystals fabricated by solvothermal treating a mixture of 0.50 g NH₄F, 2.50 mL Ti(OC₄H₉)₄ and 50 mL of glacial acetic acid at 210 °C for 24 h exhibited the highest photocatalytic activity to the decomposition of styrene. This is due to the synergistic effects of excellent crystallinity, high energy {0 0 1} crystal facets, relatively large surface area, enhanced bandgap energy and unique mesoporous structure.

© 2013 Elsevier B.V. All rights reserved.

1. Introduction

In the past few decades, nanostructured TiO₂ materials have been widely applied to many emerging research fields, such as environmental remediation and solar energy conversion [1–3]. Studies have shown that the performance of TiO₂ material is highly dependent on its size, surface area, crystal structure and exposed crystal facet [4–6]. Recently, the synthesis of anatase TiO₂ with exposed high energy {0 0 1} facet has attracted intensive research interest because both theoretical prediction and experimental results indicate that {0 0 1} crystal facet is much more reactive than other thermodynamically stable crystal facets of anatase TiO₂ [7]. However, anatase TiO₂ crystals with exposed (1 0 1) surface are more easily formed due to its much lower surface energy than that of {0 0 1} faceted surface [8]. To obtain such a highly reactive surface, it is necessary and challengeable to develop an effective method to reduce (0 0 1) surface energy [1].

In this respect, a breakthrough has been made recently by Yang et al. who, using a surface fluorination approach, have successfully synthesized well-defined anatase TiO₂ single crystals with

47% exposed {0 0 1} facets [9]. After that, enormous research work on {0 0 1} faceted anatase TiO₂ has been developed based on this surface fluorination principle [10–14]. However, it should be noted that most reported {0 0 1} faceted anatase TiO₂ single crystals were obtained by water-based synthetic strategies which usually display irregular shape and wide size distribution due to the fast nucleation and growth of TiO₂ crystals [7]. Moreover, hydrofluoric acid (HF), a dangerous and environmentally detrimental fluorine source, was frequently used in water-based method because HF plays a critical role in formation of exposed {0 0 1} crystal facets [9]. In order to avoid directly using HF, less harmful fluorine sources such as NH₄F [15,16], TiF₄ [17,18] and ion liquid containing F [19,20] have been then applied in the fabrication of anatase TiO₂ with exposed {0 0 1} facets in water-involved system. Recently, solvothermal method without addition of H₂O and HF has been an environmental benign approach to controllably grow anatase TiO₂ crystals with exposed {0 0 1} facets [7]. As reported, acetic acid is a particularly interesting candidate as a stabilizing solvent and chemical modifier of titanium alkoxides to lower the reactivity of precursors by controlling the hydrolysis of titanium precursors via slow release of H₂O through the esterification reaction between acetic acid and alcohols [21,22]. Moreover, owing to its strong chelating effect [23], acetic acid may lead to the formation of unique intermediates during solvothermal reaction and different final crystals with special morphology [22].

* Corresponding author. Tel.: +86 20 85291501; fax: +86 20 85290706.

E-mail address: antc99@gig.ac.cn (T. An).

Based on this principle, TiO_2 mesocrystals have been synthesized in the tetrabutyl titanate–acetic acid reaction system [22]. As known, mesocrystals are characterized by high crystallinity, high porosity, subunit alignment, and similarity to highly sophisticated biominerals, making them promising substitutes for single-crystalline or porous polycrystalline materials in many applications such as catalysis, sensing, and energy storage and conversion [22]. However, the obtained TiO_2 crystals do not display well-defined $\{001\}$ faceted surface. Moreover, the formation mechanism is still unclear due to the production of complex intermediates during solvothermal reaction [22]. To date, however, no matter what synthetic method is used, the fabricated $\{001\}$ faceted anatase TiO_2 as photocatalyst is mainly focused on photocatalytic degradation of organic pollutants in water [12,24], and little attention has been given to use pure anatase TiO_2 crystals with exposed $\{001\}$ reactive facets as photocatalyst for photocatalytic degradation of volatile organic compounds in air [25,26].

Herein, submicron-sized anatase TiO_2 mesocrystals with exposed $\{001\}$ surface were successfully synthesized by a facile solvothermal approach in glacial acetic acid environment. These squared-shaped mesocrystals were assembled with numerous square-shaped nanocrystals with exposed $\{001\}$ facets, leading to numerous nanopores formation and much higher surface area than reported TiO_2 single crystals with exposed $\{001\}$ surface [5]. The effects of added amount of NH_4F and solvothermal reaction time on the morphology and composition of the resulting products were investigated in detail. Further, the formed intermediates during solvothermal reaction were also identified experimentally, and a possible formation mechanism was proposed. As UV active photocatalysts, the photocatalytic activity of the prepared anatase TiO_2 mesocrystals assembled with $\{001\}$ faceted nanocrystals was evaluated in a continuous flow-through reactor by photocatalytic decomposition of gaseous styrene in air.

2. Material and methods

2.1. Synthesis

A certain amount of NH_4F (0, 0.05, 0.15, 0.30, 0.50, 0.80 and 1.20 g) was added into a dried Teflon-lined stainless-steel autoclave containing 50 mL of glacial acetic acid. After clear solution was obtained, 2.50 mL of $\text{Ti}(\text{OC}_4\text{H}_9)_4$ was introduced above mixture with stirring. Then the autoclave was heated at 210 °C for designated intervals (0.5, 1.0, 1.5, 2.0, 2.5, 3.0, 6.0, 12.0 and 24.0 h). After solvothermal reaction, the products were collected by centrifuge, washed with distilled water thoroughly and finally dried at 80 °C for 8 h. The dried samples were then calcinated at 600 °C for 90 min to remove the surface fluorine [11].

2.2. Characterizations

X-ray diffraction (XRD) patterns of the samples were recorded on a Rigaku Dmax X-ray diffractometer. The morphology and microstructure of the prepared samples were characterized by scanning electron microscope (SEM, JSM-6330F) and transmission electron microscope (TEM, JEM-2010). The ultraviolet–visible (UV–vis) absorption spectra were recorded with a UV–visible spectrophotometer (UV-2501PC). Nitrogen adsorption–desorption isotherms of the samples were obtained with a Micromeritics ASAP 2020 system.

2.3. Adsorption ability and photocatalytic activity

The adsorption capability and photocatalytic activity of the prepared samples were tested by the adsorption and degradation of

gaseous styrene with an initial concentration of $15 \pm 1 \text{ ppmv}$ operating in a same continuous flow-through mode as reported in our previous works [6,27,28]. In a typical experimental process, 0.10 g sample as photocatalyst was loaded in a cubic quartz glass reactor with a volume of $1.0 \text{ cm} \times 1.0 \text{ cm} \times 0.5 \text{ cm}$. A 365 nm UV-LED spot lamp (Shenzhen Lampic Science Co., Ltd.) was used as a light source which was fixed vertically top of the reactor with a distance of 6.0 cm (UV intensity was controlled at 70 mW cm^{-2}). Before the lamp was switched on, the gaseous styrene was allowed to reach a gas–solid adsorption equilibrium. The concentration of gaseous styrene was directly analyzed by a gas chromatograph (GC-900A) equipped with a flame ionization detector. The temperatures of the column, injector and detector were 110 °C, 230 °C and 230 °C, respectively. Gas samples were collected at regular intervals using a gas-tight locking syringe (Agilent, Australia), and a 200 μL gas sample was injected into the column for concentration determination in a splitless mode.

The adsorption efficiency and photocatalytic degradation efficiency were both calculated for styrene according to the following equation: efficiency = $(1 - C/C_0) \times 100\%$, where C is the concentration of residual pollutant, and C_0 is its original concentration.

3. Results and discussion

3.1. Structural characteristics

Fig. 1A shows the XRD patterns of the prepared sample with the added amount of 0.15 g NH_4F (curve a). As shown, there are four main diffraction peaks at $2\theta = 25.3, 37.8, 48.0$ and 55.1° which are corresponding to the (101) , (004) , (200) and (211) crystal face of anatase TiO_2 . And no other diffraction peaks can be observed, indicating that the prepared sample is anatase TiO_2 [29]. **Fig. 1B** and C shows the SEM images of the prepared anatase TiO_2 sample. It can be seen that the product consists of evenly distributed submicron-sized particle-like structures (**Fig. 1B**). Further observation indicates that these particle-like structures are square-shaped with an average side length of ca. 350 nm (**Fig. 1C**). TEM examination clearly demonstrated that the anatase TiO_2 crystal is indeed a square-shaped structure with exposed $\{001\}$ surface. Interestingly, the $\{001\}$ faceted surface of the anatase TiO_2 crystal is assembled with numerous square-shaped nanocrystals with exposed $\{001\}$ facets having side length around 10–40 nm (**Fig. 1D**). A selected area electron diffraction (SAED) pattern (top inset in **Fig. 1D**) indicates that these square-shaped nanocrystals have good crystal nature. The zone axis is $[001]$ and in turn the exposed faceted surface is the $\{001\}$ surface [13]. The corresponding high-resolution TEM image (bottom inset in **Fig. 1D**) shows the perpendicular lattice spacing of 0.19 nm representing the (200) and (020) atomic planes of anatase TiO_2 , further confirming that the exposed crystal facet of the nanocrystal is indeed the $\{001\}$ facet [30]. These exposed $\{001\}$ faceted surfaces of the nanocrystals constitute a larger $\{001\}$ surface dominated anatase TiO_2 crystal.

The effect of the added amount of NH_4F on the morphology and composition of the sample is investigated in this work. **Figs. 2 and 3** show the SEM images and XRD patterns of the samples synthesized in a reaction solution containing 50 mL glacial acetic acid, 2.5 mL $\text{Ti}(\text{OC}_4\text{H}_9)_4$ and different added amounts of NH_4F with solvothermal reaction at 210 °C for 24 h, respectively. When NH_4F is absent, spindle-shaped TiO_2 structures with about 200 nm in length and 100 nm in width are observed (**Fig. 2A**). A high-magnification SEM image (inset in **Fig. 2A**) reveals that the surface of the spindle-shaped structure is relatively rough and composed of tiny nanoparticles with diameters around 10–20 nm, which is consistent with the reported result by Ye et al. [22]. In their study, a similar TiO_2 structure is highly oriented along $[001]$ direction [22], implying

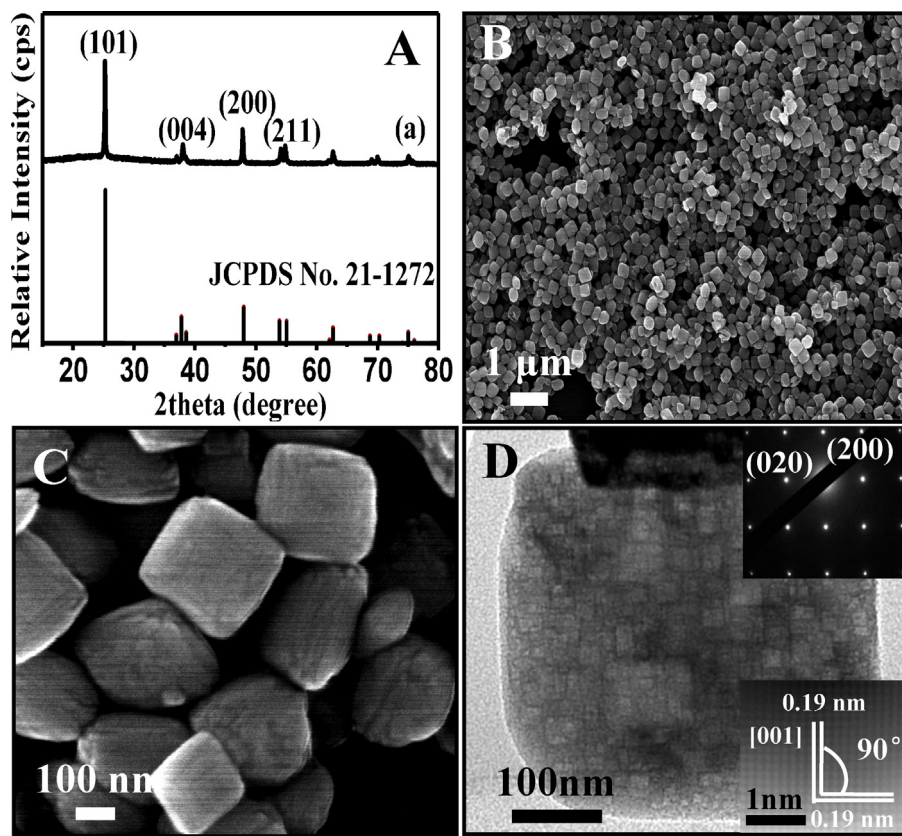


Fig. 1. (A) XRD patterns of prepared sample with the added amount of 0.15 g NH₄F (curve a) and JCPDS No. 21-1272 is used as a reference of bulk anatase TiO₂. (B) SEM image of the prepared sample (low magnification). (C) SEM image of the prepared sample (high magnification). (D) TEM image, SAED pattern (top inset) and high-resolution TEM image (bottom inset) of the prepared sample.

that {0 0 1} exposed facets are not dominant. Some spindle-shaped structures are transformed to square-shaped structures resulting in a mixture of spindle- and square-shaped structures when 0.05 g NH₄F is added (Fig. 2B). Under this condition, all obtained structures with smooth surface show larger size than that obtained without NH₄F (inset in Fig. 2B). The size increase of these structures may be due to the existence of F⁻, which can enhance the crystallization of anatase phase and promote crystallite growth [31]. The fabricated samples were further determined by XRD technique (Fig. 3). The diffraction peaks of the sample obtained with 0.05 g NH₄F is obviously stronger and sharper than those of the sample without NH₄F, implying a higher crystallinity of the former and further confirming F⁻ role in enhancing the crystallization of anatase phase. With increasing NH₄F amount to 0.15 g, spindle-shaped structures disappear and purely square-shaped structures with side length of ca. 350 nm are obtained (Fig. 1B and C). Compared to the samples obtained with 0 and 0.15 g NH₄F, the addition of NH₄F can efficiently retard the growth of the crystal structure along [0 0 1] direction, resulting in the formation of square-shaped structures with high {0 0 1} exposed faceted surface. When the added amount of NH₄F is further increased to 0.30 g (Fig. 2C), spherical-like anatase TiO₂ structures are formed which then melt together to form cluster-like and film-like structures with further increasing NH₄F amount to 0.50 and 0.80 g, respectively (Fig. 2D and E). The above results indicate that NH₄F plays an important role in controlling the morphology of the anatase TiO₂, and high quality square-shaped anatase TiO₂ crystals assembled by nanocrystals with exposed {0 0 1} facets can be only synthesized with an apt amount of NH₄F (0.15 g in this case). Moreover, it is found that the diffraction peak located at $2\theta = 37.8^\circ$ of the sample becomes much weaker and wider with increasing the added amount of NH₄F from

0.15 to 0.80 g than that of the sample obtained with 0.05 g NH₄F (Fig. 3), revealing that excessive amount of NH₄F (≥ 0.15 g) can effectively retard the oriented growth of anatase TiO₂ along [0 0 1] direction [32], leading to significantly increased {0 0 1} exposed facets [33]. When 1.20 g NH₄F is introduced into the reaction system (Figs. 2F and 3), bulky NH₄TiOF₃ particles with an average size of ca. 400 nm are formed [34,35]. Based on the above results, it can be found that the products with different morphology (from spindle shape to bulk) and composition (from TiO₂ to NH₄TiOF₃) can be easily adjusted by simply controlling the added amount of NH₄F. With an apt added amount of NH₄F (0.15 g in this study), square-shaped single-crystal-like anatase TiO₂ structures assembled by square-shaped nanocrystals with exposed {0 0 1} facets can be obtained.

3.2. N₂ adsorption-desorption isotherms

To further investigate the pore structure properties of the prepared samples, the N₂ adsorption-desorption isotherms and corresponding pore size distribution curves of the samples prepared with different added amounts of NH₄F (0, 0.15, 0.50 and 0.80 g) are plotted (Fig. 4). It can be seen that all isotherms are of type IV (IUPAC classification) with a typical H3 hysteresis loop, indicating the existence of mesoporous structure and slit-like pores [6,36,37]. The average pore sizes of the samples prepared with the added amount of 0, 0.15, 0.50 and 0.80 g NH₄F are calculated almost the same as 12.2, 10.6, 11.2 and 12.0 nm, respectively (the inset of Fig. 4). Again, these prepared samples are confirmed as mesoporous materials. Previously, it has been reported that the sample synthesized without addition of NH₄F is mesoporous material due to the existence of tiny nanoparticles on the large size structure

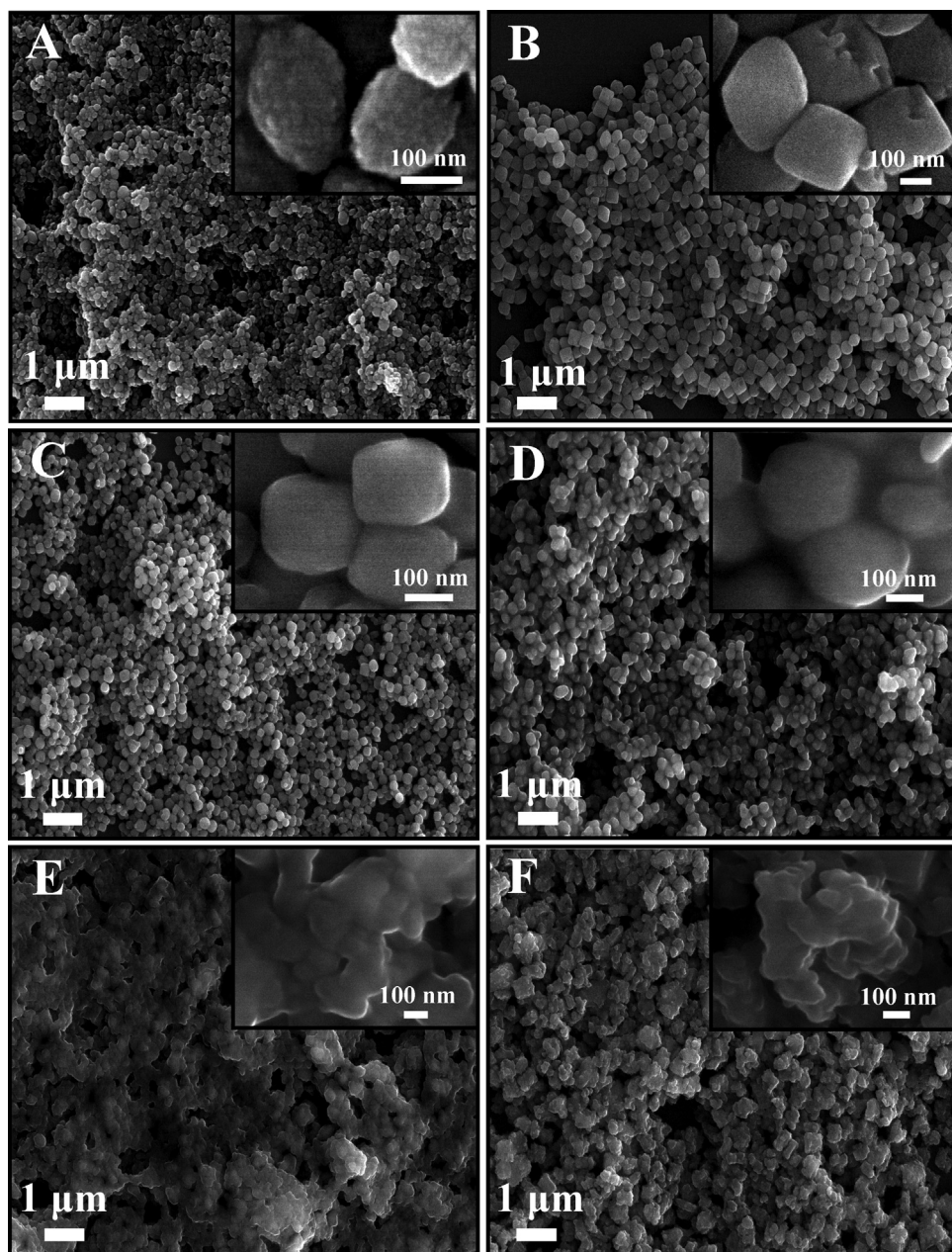


Fig. 2. SEM images of the prepared samples fabricated with different added amounts of NH₄F: (A) 0 g; (B) 0.05 g; (C) 0.30 g; (D) 0.50 g; (E) 0.80 g; and (F) 1.20 g.

[22]. In this case, from SEM and TEM results displayed above, the single-crystal-like anatase TiO₂ structures are also assembled by nanocrystals with exposed {0 0 1} facets. Thus, similar as the reported result [22], mesoporous structures can be formed between these nanocrystals after removal of the organic residuals by calcination. The quantitative details about the Brunauer–Emmett–Teller (BET) surface areas, Barrett–Joyner–Halen (BJH) total pore volumes and average pore diameter are listed in Table 1. Clearly, with increasing the added amount of NH₄F from 0 to 0.80 g, the BET surface area and the total pore volume of the samples decrease from 97.4 m²/g and 0.152 cm³/g to 18.3 m²/g and 0.041 cm³/g, respectively. Moreover, the samples prepared with the addition of NH₄F in this study show lower BET surface areas than that of P25 (surface area of 50 m²/g). Larger BET surface area and bigger total pore volume may lead to higher adsorption capacity of the TiO₂ sample on pollutants which can be verified by the results displayed in the followed adsorption experiments.

Table 1
Effect of the amount of NH₄F on structure properties of photocatalysts.

Amount of NH ₄ F(g)	BET surface area (m ² /g)	Average pore size (nm)	BJH total volume (cm ³ /g)	Relative ^a crystallinity
0	97.4	12.2	0.152	1.00
0.15	26.4	10.6	0.067	1.31
0.50	19.1	11.2	0.052	1.50
0.80	18.3	12.0	0.041	0.56

^a The relative intensity of the diffraction peak from the anatase (1 0 1) plane (reference = the sample prepared with the amount of 0 g NH₄F).

3.3. UV-vis analysis

Fig. 5 shows the UV–vis absorption spectra and the indirect band energy of the prepared photocatalysts. All samples exhibited a typical absorption with an intense transition in the UV region of the spectrum, which was attributed to the electron transition of TiO₂

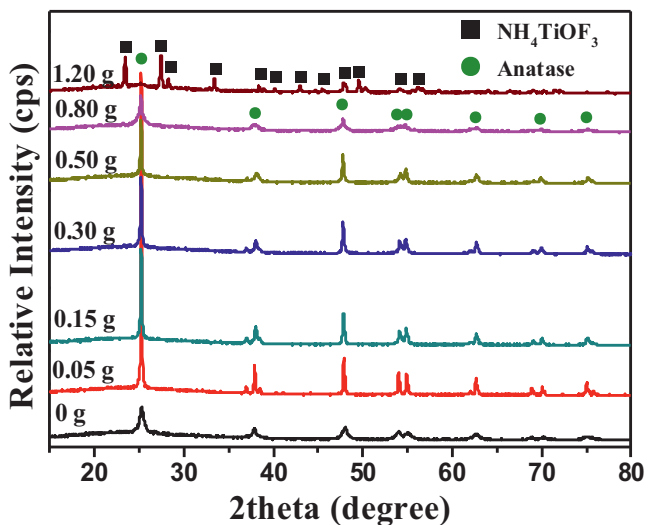


Fig. 3. XRD patterns of the prepared samples fabricated with different added amounts of NH_4F .

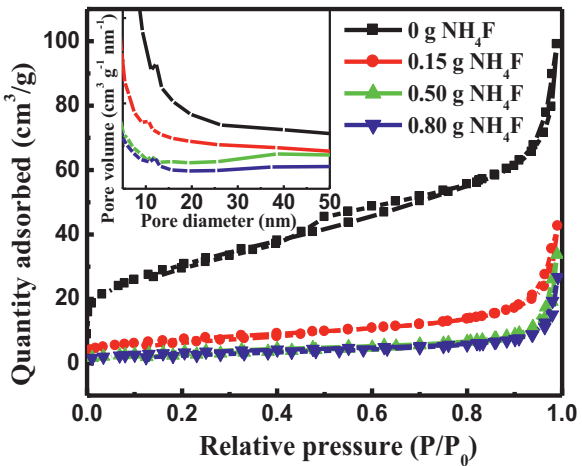


Fig. 4. N_2 adsorption–desorption isotherm and pore-size distribution curves of samples prepared with added amounts of 0, 0.15, 0.50 and 0.80 g NH_4F .

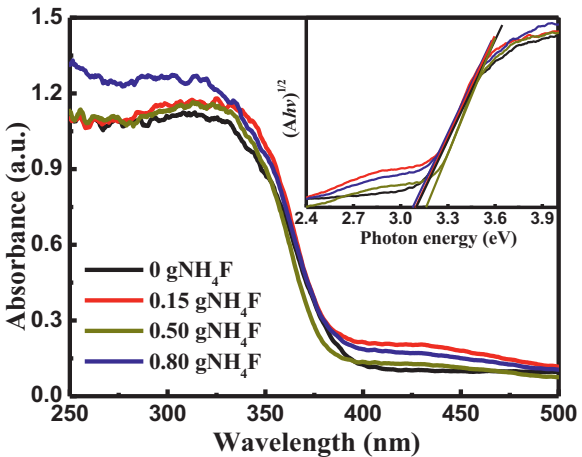


Fig. 5. UV-vis absorption spectra of the photocatalysts obtained with addition of different amounts of NH_4F .

from the valence band to the conduction band [38]. The indirect band gap energies of the prepared samples were estimated from a plot of $(\alpha h\nu)^{1/2}$ versus photon energy ($h\nu$) (inset in Fig. 5). The intercept of the tangent to the plot gave a good approximation of the indirect bandgap energy of the fabricated anatase TiO_2 . The absorption coefficient α could be calculated from the absorbance. From the inset in Fig. 5, the indirect band gap energies estimated from the intercept of the tangents to the plots are 3.09, 3.08, 3.14 and 3.09 eV for the prepared photocatalysts obtained with the added amounts of 0, 0.15, 0.50 and 0.80 g NH_4F , respectively. It can be seen that a wider bandgap is clearly observed for the sample obtained with 0.50 g NH_4F , possibly owing to the presence of surface tiny nanocrystals. The large bandgap may mean that the fabricated TiO_2 sample has stronger redox ability during photocatalytic reaction [39].

3.4. Formation mechanism

To investigate the growth mechanism, the growth processes of TiO_2 submicron-sized mesocrystal are examined in detail by SEM and XRD techniques. Fig. 6 shows the SEM images of the as-synthesized samples with different reaction times (the added amount of 0.15 g NH_4F for all investigated samples). It can be seen that with 0.5 h of solvothermal treatment, the particulate products with irregular shape having particle size ranging from 50 to 150 nm are formed (Fig. 6A), which then melt together to form film-like structure after 1.0 h of solvothermal treatment (Fig. 6B) and further transform to nanofibers when the reaction time prolongs to 1.5 h (Fig. 6C). After solvothermal treatment of 2.0 h, a mixture of nanofibers and particles can be observed (Fig. 6D), and the particles become dominant after 2.5 h (Fig. 6E). Then, the formed particles with irregular shape further evolve into square-shaped structures and the co-existed nanofibers are totally transformed into particle clusters when the reaction time further increases to 3.0 h (Fig. 6F). Finally, these particle clusters dissolve and grow slowly to form square-shaped structures, as shown in Fig. 6G and H with extending the reaction time continuously to 6.0 and 12.0 h, and high quality square-shaped TiO_2 submicron-sized crystals are obtained after 24.0 h of reaction and then mesocrystals are synthesized after calcination.

Besides the morphology evolution, the composition of the products obtained at different reaction times is correspondingly investigated. Fig. 7 shows the XRD data of the as-prepared products from different reaction times. Clearly, the XRD patterns of sample obtained with 0.5 h of solvothermal reaction is a mixture of NH_4TiOF_3 and anatase TiO_2 diffraction peaks. As the treatment time increases to 1.0 h, the intensity of NH_4TiOF_3 diffraction peaks weakens dramatically. Moreover, the diffraction peak intensity of the NH_4TiOF_3 becomes weaker and weaker with the reaction time further increasing and finally disappears when the reaction time reaches 3.0 h. On the contrary, the intensity of diffraction peaks for anatase TiO_2 become much stronger when the treatment time increases and the XRD patterns obtained from the samples treated for 3.0–24 h can be indexed to pure anatase TiO_2 . The XRD results further support the morphology change of the fabricated samples, suggesting a four-stage formation process as shown in Scheme 1: (1) formation of a mixture of NH_4TiOF_3 and anatase TiO_2 (0–0.5 h) (step A); (2) dissolution and rearrangement of NH_4TiOF_3 to form anatase TiO_2 (0.5–3.0 h) (steps B–E); (3) growth of square-shaped anatase TiO_2 crystals (3.0–24 h) (step F) and (4) subsequent calcination to obtain TiO_2 mesocrystal (step G). Therefore, a tentative formation mechanism of TiO_2 submicron-sized single-crystal-like mesocrystals obtained by solvothermal method is proposed and illustrated as follows: firstly, $\text{Ti}(\text{OC}_4\text{H}_9)_4$ reacts with glacial acetic acid to release $\text{C}_4\text{H}_9\text{OH}$ [22]. The produced $\text{C}_4\text{H}_9\text{OH}$ then reacts with the glacial acetic acid to form water by a slow

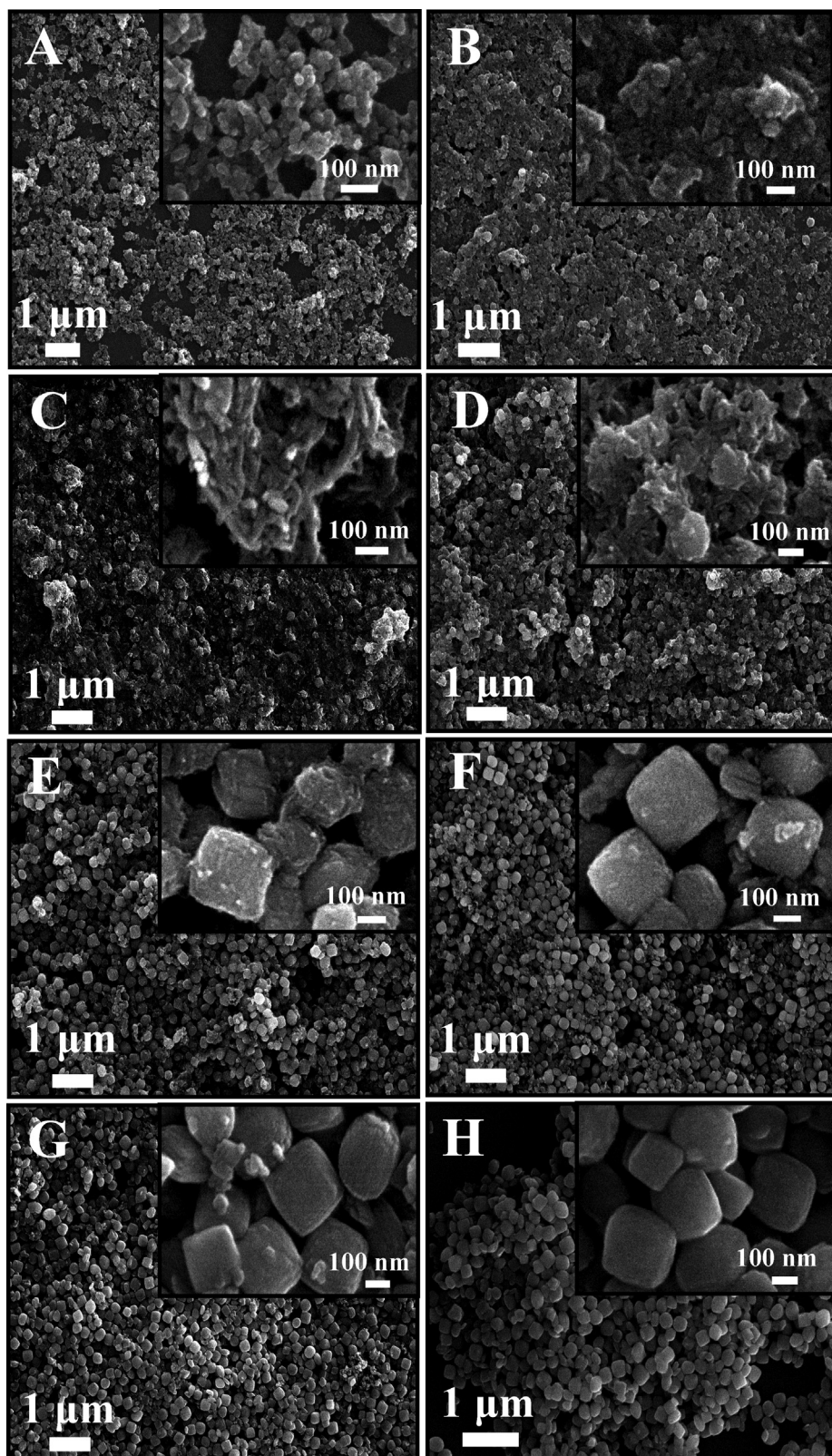


Fig. 6. SEM images of the prepared samples fabricated with different reaction times: (A) 0.5 h; (B) 1.0 h; (C) 1.5 h; (D) 2.0 h; (E) 2.5 h; (F) 3.0 h; (G) 6.0 h; and (H) 12.0 h.

esterification reaction (Eq. (1)). Subsequently, hydrolysis reaction occurs for $\text{Ti}(\text{OC}_4\text{H}_9)_4$ to form $\text{Ti}(\text{OH})_4$ (Eq. (2)), further forming TiO_2 growth seeds (Eq. (3)). Meanwhile, HF is generated through the hydrolysis of NH_4F (Eq. (4)). Then OH^- on the surface of TiO_2 growth seeds will be substituted by F^- to form TiF_6^{2-} (Eq. (5)), further

producing $[\text{TiF}_3(\text{OH})_3]^{2-}$ (Eq. (6)). Then, NH_4TiOF_3 is formed after reaction with NH_4^+ under the acidic environment (Eq. (7)) [35]. The formation of the anatase involves the dissolution of ammonium and fluoride ions from the NH_4TiOF_3 , followed by collapse to anatase [35]. Finally, anatase TiO_2 mesocrystals with preserved

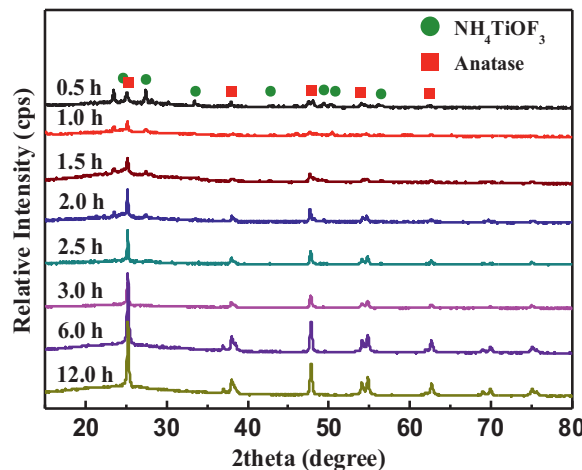
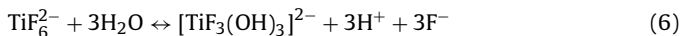
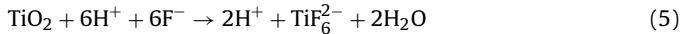
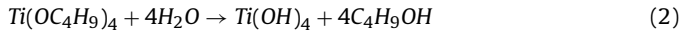
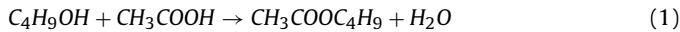


Fig. 7. XRD patterns of the prepared samples fabricated with different reaction times.

morphology can be obtained after removal of the organic residuals by subsequent calcination, accompanied by a moderate increase in the size of the nanocrystals [22].



3.5. Adsorption capability and photocatalytic activity

Fig. 8 shows the adsorption, direct photolysis and photocatalytic decomposition curves of gaseous styrene by the anatase TiO_2 photocatalysts prepared with different NH_4F amounts. For comparison, commercially available P25 was also measured by

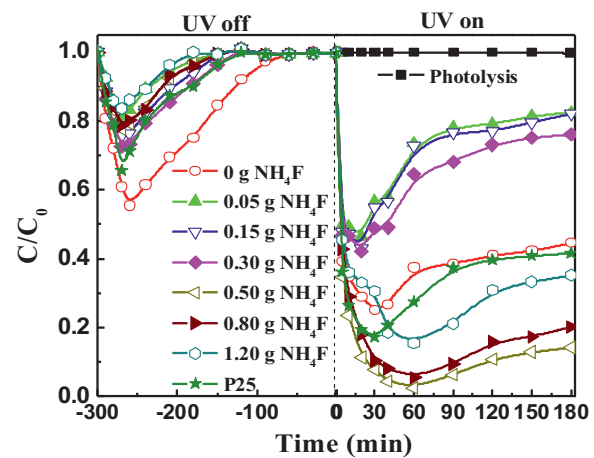
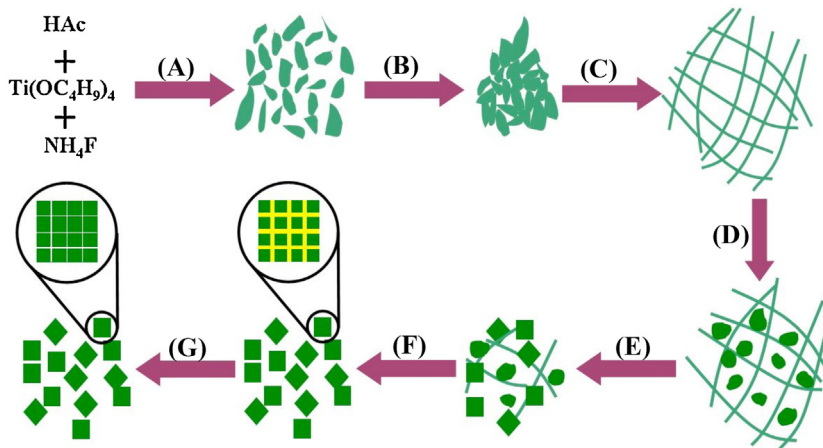


Fig. 8. Adsorption, photolysis and photocatalytic degradation kinetic curves of styrene by P25 and photocatalysts prepared with different added amounts of NH_4F .

photocatalytic decomposition of gaseous styrene. Before switching on the lamp, the adsorption equilibrium experiments were firstly conducted. From **Fig. 8**, styrene is swiftly adsorbed onto all investigated samples during the initial 20–30 min until slow breakthrough occurs (breakthrough point is defined here where the outlet concentration of styrene is equal to 5% of the inlet styrene concentration). For P25, the complete breakthrough (when the outlet and inlet concentrations of styrene are equal) is observed after 180 min of adsorption. Similar result can be also found for the sample prepared with the added amount of 0.30 g NH_4F . For samples obtained with the added NH_4F amount of 0.05, 0.15, 0.50 and 0.80 g, the complete breakthrough time is the same (150 min) which is shorter than that of P25. Moreover, the synthesized samples with the added NH_4F amount of 0 (270 min) and 1.20 g (120 min) show the highest and lowest adsorption capacities to styrene, respectively. Clearly, the time for complete breakthrough follows the order: 1.20 g NH_4F < 0.80 g NH_4F = 0.50 g NH_4F = 0.15 g NH_4F = 0.05 g NH_4F < P25 = 0.30 g NH_4F < 0 g NH_4F . This result indicates that all samples prepared with the addition of NH_4F show similar adsorption capability as that for P25 due to their unique mesoporous structure, while the sample obtained in the absent of NH_4F shows the highest adsorption ability which is consistent with the BET surface area results.

As the adsorption equilibrium reached, the lamp is switched on. Firstly, the control experiment of direct photolysis is carried out, and less than 1% of styrene is removed after 180 min



Scheme 1. Schematic illustration of the formation mechanism for the anatase TiO_2 mesocrystals with exposed (0 0 1) surface.

of photolysis, indicating that only UV light cannot efficiently decompose the styrene. When photocatalyst is present, different removal efficiencies are observed for various photocatalysts. For P25, a swift removal of styrene (82.9%) can be discerned in the first 30 min. However, as UV illumination goes on for another 60 min, the decomposition efficiency decreases sharply to 62.6%, which can be ascribed to the blockage of photocatalytic active sites by stable intermediates on the TiO₂ surface during the photocatalytic removal of styrene, thereby leading to the decrease of the photocatalytic efficiency [38,40]. Finally, a steady state with the decomposition efficiency of ca. 58.5% is achieved [41]. For all prepared photocatalysts in this study, similar decomposition curve to P25 is obtained as reported in our previous works [6,28]. After 180 min of photocatalytic reaction, the decomposition efficiencies follow the order: 0.05 g NH₄F (17.5%) < 0.15 g NH₄F (17.9%) < 0.03 g NH₄F (23.4%) < 0 g NH₄F (55.5%) < P25 (58.5%) < 1.20 g NH₄F (64.9%) < 0.80 g NH₄F (79.9%) < 0.50 g NH₄F (85.9%). Apparently, the sample obtained with the added amount of 0.50 g NH₄F shows the best photocatalytic activity.

This enhanced photocatalytic activity may be attributed to the synergistic effects of several factors such as relative crystallinity, band energy, specific surface area, high percentage of {001} facets and mesoporous structure. Relative crystallinity is an important factor influencing the photocatalytic activity of TiO₂. As shown in Table 1, the relative anatase crystallinity increases sharply from 1.00 to 1.50 for the samples prepared with the increase of the added amount of NH₄F from 0 to 0.50 g. The relative anatase crystallinity then decreases to 0.56 for the samples prepared with the added amounts of 0.80 g NH₄F. In the case of specific surface area, this sample does not display the largest specific surface area among the prepared samples. However, it has already been proved that large surface area is not the only decisive factor for the enhancement of the photocatalytic activity of TiO₂ photocatalyst because TiO₂ with a large surface area is usually accompanied by a large number of crystalline defects, which could act as the centers for the recombination of photogenerated electrons and holes, leading to poor photoactivity of TiO₂ [39,42]. Moreover, high percentage of {001} facets also plays an important role. Previous study has shown that the photocatalytic efficiency increases with the increase of percentage of {001} facets for anatase TiO₂ [43]. Furthermore, the unique mesoporous structure of each particle will facilitate the transfer and diffusion of styrene molecules in the catalyst. Thus, the photocatalyst sample prepared with the added amount of 0.50 g NH₄F shows the highest photocatalytic activity in this study due to the relatively large surface area, which can efficiently enrich reactant molecules, and good anatase crystallinity as well as high percentage of {001} facets, which can reduce the electron and hole recombination [43,44]. Much wider band energy can result in the photocatalyst with high redox capability and the unique mesoporous structure can facilitate the transfer and diffusion of styrene molecules. All these factors combined together are responsible for the highest photocatalytic activity of the sample prepared with the added amount of 0.50 g NH₄F.

4. Conclusions

TiO₂ submicron-sized mesocrystal photocatalyst with exposed {001} surface has been successfully synthesized by a facile solvothermal method. The results revealed that the added amount of NH₄F and solvothermal reaction time played both significant roles in the formation of the TiO₂ submicron-sized mesocrystal structure. Formation of the mixed NH₄TiOF₃ and anatase TiO₂, dissolution and transformation of NH₄TiOF₃ to anatase TiO₂, growth process of TiO₂ submicron-sized crystal assembled by nanocrystals with {001} exposed facets and subsequent calcination to obtain

TiO₂ mesocrystal were found to be four major synthesis stages. The photocatalytic degradation results revealed that the photocatalyst prepared when 0.50 g NH₄F as well as 2.50 mL Ti(OC₄H₉)₄ added to 50 mL of glacial acetic acid and then solvothermally treated for 24 h at 210 °C showed the highest photocatalytic activity in the decomposition of gaseous styrene, due to the synergistic effects of its good anatase crystallinity, high percentage of {001} facets, relatively large surface area, wide band energy and unique mesoporous structure.

Acknowledgements

This is contribution No. 1757 from GIGCAS. This work was partially supported by the Science and Technology Project of Guangdong Province, China (2011A030700003 and 2012A032300017), the Cooperation Projects of the Chinese Academy of Science with Foshan Government (20121071010041), Team Project of Natural Science Foundation of Guangdong Province, China (S2012030006604) and National Nature Science Foundation of China (21077104).

References

- [1] P.R. Liu, Y. Wang, H.M. Zhang, T.C. An, H.G. Yang, Z.Y. Tang, W.P. Cai, H.J. Zhao, *Small* 8 (2012) 3664–3673.
- [2] J.Y. Chen, X.L. Liu, G.Y. Li, X. Nie, T.C. An, S.Q. Zhang, H.J. Zhao, *Catal. Today* 164 (2011) 364–369.
- [3] K. Maeda, K. Teramura, D.L. Lu, T. Takata, N. Saito, Y. Inoue, K. Domen, *Nature* 440 (2006) 295.
- [4] Z.Y. Wang, K.L. Lv, G.H. Wang, K.J. Deng, D.G. Tang, *Appl. Catal., B* 100 (2010) 378–385.
- [5] Z.C. Lai, F. Peng, Y. Wang, H.J. Wang, H. Yu, P.R. Liu, H.J. Zhao, *J. Mater. Chem.* 22 (2012) 23906–23912.
- [6] T.C. An, J.Y. Chen, X. Nie, G.Y. Li, H.M. Zhang, X.L. Liu, H.J. Zhao, *ACS Appl. Mater. Interfaces* 4 (2012) 5988–5996.
- [7] J.A. Zhu, S.H. Wang, Z.F. Bian, S.H. Xie, C.L. Cai, J.G. Wang, H.G. Yang, H.X. Li, *CrystEngComm* 12 (2010) 2219–2224.
- [8] M. Lazzeri, A. Vittadini, A. Selloni, *Phys. Rev. B* 63 (2001) 155409.
- [9] H.G. Yang, C.H. Sun, S.Z. Qiao, J. Zou, G. Liu, S.C. Smith, H.M. Cheng, G.Q. Lu, *Nature* 453 (2008) 638–U634.
- [10] J. Pan, G. Liu, G.M. Lu, H.M. Cheng, *Angew. Chem. Int. Ed.* 50 (2011) 2133–2137.
- [11] H.G. Yang, G. Liu, S.Z. Qiao, C.H. Sun, Y.G. Jin, S.C. Smith, J. Zou, H.M. Cheng, G.Q. Lu, *J. Am. Chem. Soc.* 131 (2009) 4078–4083.
- [12] X.G. Han, Q. Kuang, M.S. Jin, Z.X. Xie, L.S. Zheng, *J. Am. Chem. Soc.* 131 (2009) 3152.
- [13] H.M. Zhang, Y.H. Han, X.L. Liu, P.R. Liu, H. Yu, S.Q. Zhang, X.D. Yao, H.J. Zhao, *Chem. Commun.* 46 (2010) 8395–8397.
- [14] C.Z. Wen, H.B. Jiang, S.Z. Qiao, H.G. Yang, G.Q. Lu, *J. Mater. Chem.* 21 (2011) 7052–7061.
- [15] W.Q. Wu, H.S. Rao, Y.F. Xu, Y.F. Wang, C.Y. Su, D.B. Kuang, *Sci. Rep.* 3 (2013) 1892.
- [16] D.P. Wu, Z.Y. Gao, F. Xu, J.L. Chang, S.Y. Gao, K. Jiang, *CrystEngComm* 15 (2013) 516–523.
- [17] J.W. Miao, B. Liu, *RSC Adv.* 3 (2013) 1222–1226.
- [18] J.G. Wang, P. Zhang, X. Li, J. Zhu, H.X. Li, *Appl. Catal., B* 134 (2013) 198–204.
- [19] D.Q. Zhang, M.C. Wen, P. Zhang, J. Zhu, G.S. Li, H.X. Li, *Langmuir* 28 (2012) 4543–4547.
- [20] J.F. Lei, K. Du, R.H. Wei, J. Ni, L.B. Li, W.S. Li, *RSC Adv.* 3 (2013) 13843–13850.
- [21] J.K. Liu, T.C. An, G.Y. Li, N.Z. Bao, G.Y. Sheng, J.M. Fu, *Microporous Mesoporous Mater.* 124 (2009) 197–203.
- [22] J.F. Ye, W. Liu, J.G. Cai, S.A. Chen, X.W. Zhao, H.H. Zhou, L.M. Qi, *J. Am. Chem. Soc.* 133 (2011) 933–940.
- [23] D.P. Birnie, N.J. Bendzko, *Mater. Chem. Phys.* 59 (1999) 26–35.
- [24] D.Q. Zhang, G.S. Li, X.F. Yang, J.C. Yu, *Chem. Commun.* (2009) 4381–4383.
- [25] M.V. Sofianou, V. Psycharidis, N. Boukos, T. Vaimakis, J.G. Yu, R. Dillert, D. Bahne-mann, C. Trapalis, *Appl. Catal., B* 142 (2013) 761–768.
- [26] M.V. Sofianou, C. Trapalis, V. Psycharidis, N. Boukos, T. Vaimakis, J.G. Yu, W.G. Wang, *Environ. Sci. Pollut. Res. Int.* 19 (2012) 3719–3726.
- [27] J.Y. Chen, G.Y. Li, Y. Huang, H.M. Zhang, H.J. Zhao, T.C. An, *Appl. Catal., B* 123–124 (2012) 69–77.
- [28] J.Y. Chen, X. Nie, H.X. Shi, G.Y. Li, T.C. An, *Chem. Eng. J.* 228 (2013) 834–842.
- [29] X.H. Yang, Z. Li, G. Liu, J. Xing, C.H. Sun, H.G. Yang, C.Z. Li, *CrystEngComm* 13 (2011) 1378–1383.
- [30] H.M. Zhang, P.R. Liu, F. Li, H.W. Liu, Y. Wang, S.Q. Zhang, M.X. Guo, H.M. Cheng, H.J. Zhao, *Chem. Eur. J.* 17 (2011) 5949–5957.
- [31] J.G. Yu, J. Zhang, *Dalton Trans.* 39 (2010) 5860–5867.
- [32] X.H. Yang, Z. Li, C.H. Sun, H.G. Yang, C.Z. Li, *Chem. Mater.* 23 (2011) 3486–3494.
- [33] N. Roy, Y. Sohn, D. Pradhan, *ACS Nano* 7 (2013) 2532–2540.

- [34] N.M. Laptash, I.G. Maslennikova, T.A. Kaidalova, *J. Fluorine Chem.* 99 (1999) 133–137.
- [35] L. Zhou, D. Smyth-Boyle, P. O'Brien, *J. Am. Chem. Soc.* 130 (2008) 1309–1320.
- [36] M. Kruk, M. Jaroniec, *Chem. Mater.* 13 (2001) 3169–3183.
- [37] T.C. An, J.K. Liu, G.Y. Li, S.Q. Zhang, H.J. Zhao, X.Y. Zeng, G.Y. Sheng, J.M. Fu, *Appl. Catal., A* 350 (2008) 237–243.
- [38] Y.J. Xu, Y.B. Zhuang, X.Z. Fu, *J. Phys. Chem. C* 114 (2010) 2669–2676.
- [39] M.H. Zhou, J.G. Yu, S.W. Liu, P.C. Zhai, B.B. Huang, *Appl. Catal., B* 89 (2009) 160–166.
- [40] R. Mendez-Roman, N. Cardona-Martinez, *Catal. Today* 40 (1998) 353–365.
- [41] T.C. An, M.L. Zhang, X.M. Wang, G.Y. Sheng, J.M. Fu, *J. Chem. Technol. Biotechnol.* 80 (2005) 251–258.
- [42] K. Tanaka, M.F.V. Capule, T. Hisanaga, *Chem. Phys. Lett.* 187 (1991) 73–76.
- [43] X.G. Han, X. Wang, S.F. Xie, Q. Kuang, J.J. Ouyang, Z.X. Xie, L.S. Zheng, *RSC Adv.* 2 (2012) 3251–3253.
- [44] T. Tachikawa, S. Yamashita, T. Majima, *J. Am. Chem. Soc.* 133 (2011) 7197–7204.